Int. J. Electrochem. Sci., 10 **(2015)** 3282 - 3290

International Journal of
ELECTROCHEMICAL
SCIENCE
www.electrochemsci.org

Short Communication

Advances in Direct Formic Acid Fuel Cells: Fabrication of Efficient Ir/Pd Nanocatalysts for Formic Acid Electro-Oxidation

Islam M. Al-Akraa[1,*], *Ahmad M. Mohammad*[1,2], *Mohamed S. El-Deab*[2,*], *Bahgat E. El-Anadouli*[2]

[1]Chemical Engineering Department, Faculty of Engineering, British University in Egypt, Cairo, Egypt
[2] Chemistry Department, Faculty of Science, Cairo University, Cairo, Egypt
[*]E-mail: islam.ahmed@bue.edu.eg; msaada68@yahoo.com

Received: 11 December 2014 / *Accepted:* 14 January 2015 / *Published:* 24 February 2015

The modification of a glassy carbon (GC) electrode with palladium (PdNPs) and Iridium (IrNPs) nanoparticles is targeted to develop efficient anodes for formic acid electro–oxidation (FAO). The deposition order of PdNPs and IrNPs is appropriately adjusted in such a way that could improve the electrocatalytic activity and stability of the electrode towards FAO. The highest catalytic activity and stability are obtained at the Ir/Pd/GC electrode (with PdNPs directly deposited onto the GC electrode followed with IrNPs). Such enhancement is manifested in the increase of the oxidation current of formic acid (FA) together with a favorable negative shift in the onset potential of FAO. This marvelous enhancement is believed to originate from the electronic enhancement and/or the bi-functional mechanism of IrNPs to the Pd–based catalysts.

Keywords: Electrocatalysis; Fuel cells; Formic acid electro-oxidation; Stability; Palladium; Iridium

1. INTRODUCTION

Environmental hazards and limitations of fossil fuels have drawn the global community's attention to replace such traditional fuels with other clean energy sources [1,2]. Of these clean energy sources, fuel cells are among the promising candidates that proved efficient, eco-friendly, reliable, quiet, long-lasted, easily installed and moved, perfect for residential and transportation uses as well as portable electronic applications [3-5]. Direct formic acid fuel cells (DFAFCs) have many advantages over the direct methanol fuel cells (MFCs) [6-8]. For instance, methanol is a toxic, evaporable, and flammable compound with high crossover through Nafion–based membranes [9]. On the other hand, Formic acid (FA) is non-toxic, non-flammable, and has a smaller crossover flux through Nafion membranes, which permits the use of high concentrated fuel solutions and thinner membranes in DFAFCs [10,11]. However, DFAFCs experience a gradual deterioration for the catalytic activity of the

Pt–based anodic catalyst that is frequently used for FA electro–oxidation (FAO). This actually happened as a consequence of the adsorption of the poisoning CO resulting from the "*non-faradaic*" dissociation of FA at Pt surface [6,7,12,13]. Therefore, overcoming this poisoning is essential in order to introduce a reliable and stable anodic catalyst for DFAFCs. Pd represents the reference catalyst for FAO where it provides even a better catalytic enhancement than Pt–based materials [14,15]. However, unfortunately, Pd catalysts suffer from a gradual deactivation with time, which remained a serious complication for their viable applications [16,17]. This deactivation was believed to originate from the adsorption of some CO–like poisoning species at the Pd surface or the dissolution of Pd under highly oxidizing conditions [18-21]. Improvement of the catalytic activity and stability of Pd catalysts towards FAO is recently sought by doping Pd with other metal and/or metal oxide promoters that have the ability to minimize the adsorption of these poisoning species and/or the rate of Pd dissolution [22,23].

In this work, an easy way is introduced for the development of an efficient and stable nanoparticle–based Ir/Pd/GC electrode (in which Pd nanoparticles (PdNPs) is directly deposited onto the GC electrode followed by Ir nanoparticles (IrNPs) deposition) for FAO. Field-emission scanning electron microscopy (FE-SEM), energy dispersive X-ray spectrometer (EDS), and X-ray diffraction (XRD) spectroscopy are used to depict the surface morphology, composition, and crystal structure of the catalyst, respectively. Furthermore, the electrochemical measurements assisted in exploring its catalytic performance.

2. EXPERIMENTAL

A freshly–prepared glassy carbon electrode (GC, ϕ = 3.0 mm) is used as a working electrode. An Ag/AgCl/KCl(sat) and a spiral Pt wire are used as the reference and counter electrodes, respectively. The electrodeposition of PdNPs is carried out in 0.1 M H_2SO_4 solution containing 1.0 mM $Pd(CH_3COO)_2$ by applying a constant potential electrolysis at 0 V for 180 s (resulting in a loading of 9.1 $\mu g\ cm^{-2}$) whereas the electrodeposition of IrNPs is carried out in 0.1 M H_2SO_4 solution containing 1.0 mM $IrCl_3$ by applying a constant potential electrolysis at –0.5 V for 60 s (resulting in a loading of 4.9 $\mu g\ cm^{-2}$).

The electrocatalytic activity of the modified electrodes toward FAO is examined in an aqueous solution of 0.3 M FA solution (pH = 3.5). The pH was adjusted by adding a proper amount of NaOH. At this pH an appreciable amount of FA is ionized to formate anion (about one third). This would enhance the ionic conductivity in the solution, thus reduces the polarization resistance, in addition to compressing the thickness of the diffusion layer [24].

The electrochemical measurements are carried ou at room temperature (25 ± 1^oC) in a two-compartment three-electrode glass cell. The measurements are performed using an EG&G potentiostat (model 273A). Current densities were calculated on the basis of the real surface area of the PdNPs (active ingredient).

A field emission scanning electron microscope, FE-SEM, (QUANTA FEG 250) coupled with an energy dispersive X-ray spectrometer (EDS) is employed to disclose the electrode's morphology

and its bulk composition. The crystallographic structure of the modified catalysts is revealed using X-ray diffraction (XRD, PANalytical, X'Pert PRO) operated with Cu target (λ=1.54Å).

3. RESULTS AND DISCUSSION

3.1. Electrochemical and materials characterization

Fig. 1 shows cyclic voltammograms (CVs) measured in Ar–saturated 0.5 M H_2SO_4 for (a) Pd/GC, (b) Ir/GC, (c) Pd/Ir/GC, and (d) Ir/Pd/GC electrodes. Fig. 1a (Pd/GC electrode) shows the typical response characterizing Pd surfaces. That is, the surface oxidation, extending over a wide range of potential, is coupled with the reduction peak at ca. 0.45 V. In addition, the hydrogen adsorption/desorption ($H_{ads/des}$) peaks appeared in the potential range from 0.0 to –0.2 V. Whereas Fig. 2b (Ir/GC electrode) shows no significant response under the prevailing experimental conditions [25].

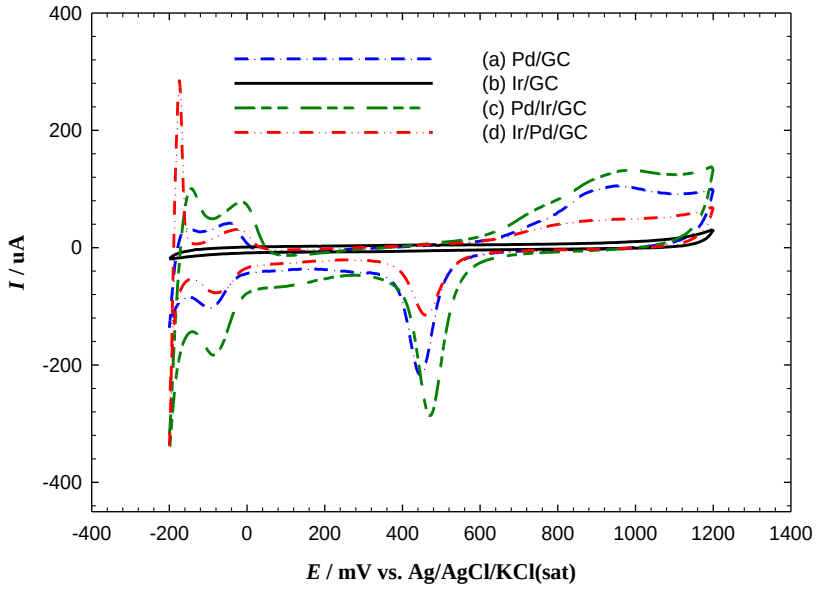

Figure 1. CVs obtained at (a) Pd/GC, (b) Ir/GC, (c) Pd/Ir/GC, and (d) Ir/Pd/GC electrodes in Ar-saturated 0.5 M H_2SO_4. Potential scan rate: 200 mVs^{-1}.

Interestingly, Fig. 1c (Pd/Ir/GC electrode) depicts an increase in the intensity of the Pd oxide reduction (at ca. 0.45 V) in comparison to that of the Pd/GC electrode (Fig. 1a). This can also be noticed in the Pd oxide formation and the $H_{ads/des}$ peaks of the Pd/Ir/GC modified electrode. This is actually predictable as the deposition of IrNPs on the GC surface can provide more active sites for the deposition of PdNPs, hence increasing the overall surface area of Pd.

On the other hand, when IrNPs are deposited onto the Pd/GC electrode (Fig. 1d), the exposed surface area of PdNPs could be seen to decrease (compare Figs. 1d and 1a) reflecting a partial coverage ($\theta \approx 30$ %) of IrNPs onto the PdNPs.

Moreover, the reduction peak of Pd oxide observed for the Pd/Ir/GC and Ir/Pd/GC electrodes reveals an anodic shift compared with that observed for Pd/GC electrode. This indicates an easier removal of adsorbed oxygen species from Pd/Ir/GC and Ir/Pd/GC electrodes compared with that from Pd/GC electrode.

Morphologically, Fig. 2 shows FE-SEM micrographs of the Pd/GC, and Ir/Pd/GC electrodes. It depicts that both catalysts have spherical lumps–based structure with an average particle size of ca.75 nm and 90 nm, respectively, for the Pd/GC (image a of Fig. 2) and the Ir/Pd/GC (image b of Fig. 2) catalysts. The EDS analysis of the Pd/GC, and Ir/Pd/GC electrodes confirmed the deposition of the different ingredients in the catalyst and assisted in calculation of their relative ratios (see Fig. 3).

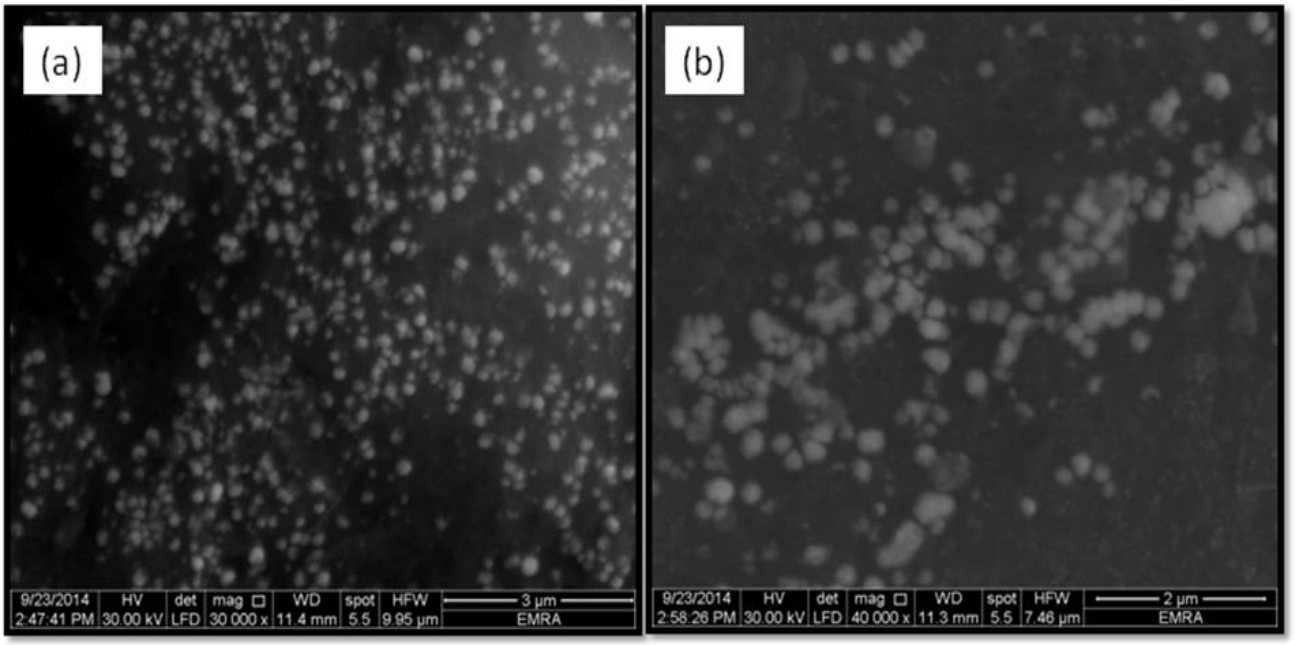

Figure 2. FE-SEM micrographs of (a) Pd/GC, and (b) Ir/Pd/GC electrodes. The electrodeposition conditions are listed in the experimental section.

The crystal structure of the Pd/GC and Ir/Pd/GC electrodes is depicted by utilizing the XRD technique. Fig. 4a (Pd/GC electrode) shows several diffraction peaks are identified at ca. 25º, 39º, 43º, and 78º corresponding, respectively, to the (002) plane of C [26], (111), (200), and (311) planes of Pd face–centered cubic (fcc) lattice [27,28].

Fascinatingly, the XRD pattern of the Ir/Pd/GC electrode (Fig. 4b) is almost the same as of the Pd/GC electrode (Fig. 4a) where no peaks related to Ir was observed. This indicates that Ir has entered into the Pd lattice and an alloy might be formed [25].

3.2. Formic acid electro-oxidation

Fig. 5 shows linear sweep voltammograms (LSVs) of FAO at the Pd/GC, Pd/Ir/GC, and Ir/Pd/GC electrodes in a 0.3 M aqueous solution of FA (pH = 3.5).

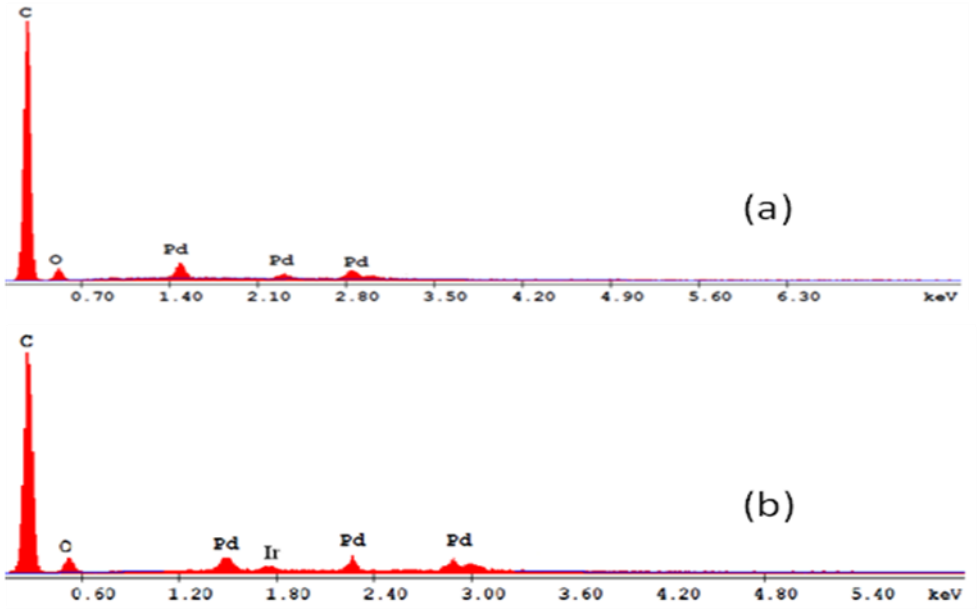

Figure 3. EDS analysis of (a) Pd/GC, and (b) Ir/Pd/GC electrodes. The electrodeposition conditions are listed in the experimental section.

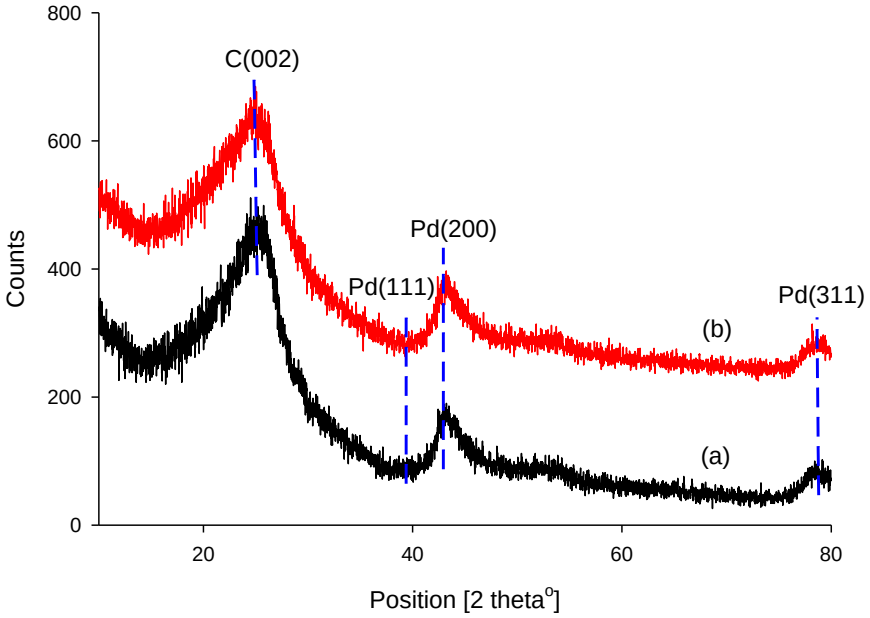

Figure 4. XRD patterns of (a) Pd/GC, and (b) Ir/Pd/GC electrodes. The electrodeposition conditions are listed in the experimental section.

It is valuable to mention here that no anodic peak is observed for FAO at the Ir/GC electrode under the experimental conditions studied herein indicating no electrocatalytic activity for this electrode towards FAO. Whereas, the reaction pathway of FAO on the Pd/GC electrode (Fig. 5a) proceeds exclusively via the dehydrogenation route in which CO_2 is the oxidation product with insignificant contribution of Pd poisoning by CO [29,30]. This is evident from the appearance of a single oxidation peak around ca. 0 V, which assigns the direct oxidation of FA to CO_2.

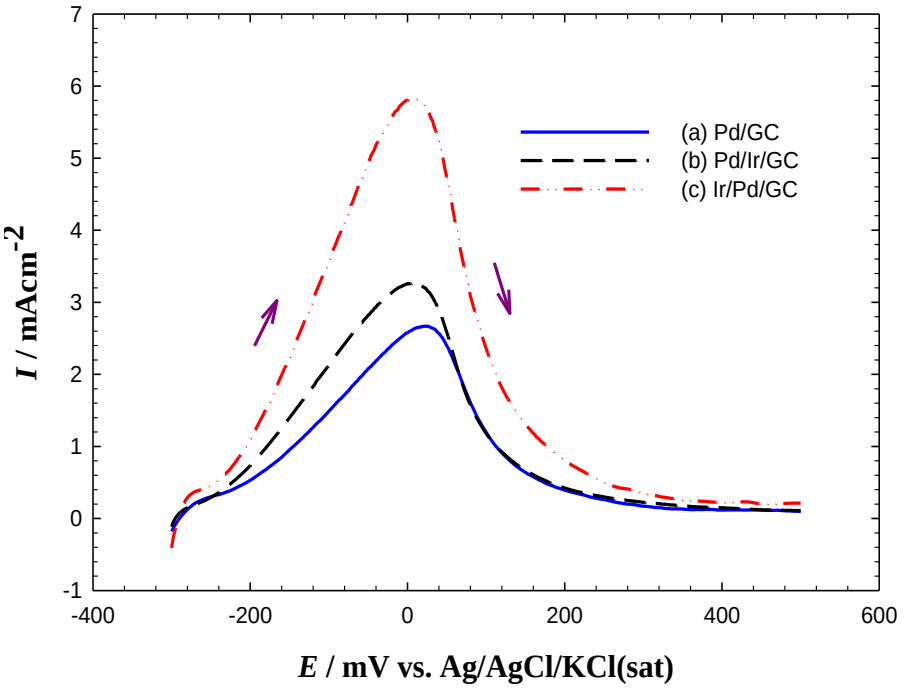

Figure 5. LSVs obtained at (a) Pd/GC, (b) Pd/Ir/GC, and (c) Ir/Pd/GC electrodes in 0.3 M HCOOH (pH = 3.5). Potential scan rate: 100 mVs^{-1}.

Interestingly, at the Pd/Ir/GC (Fig. 5b) and Ir/Pd/GC (Fig. 5c) electrodes, the peak current densities (I_p) increase to more than two folds in the case of Ir/Pd/GC electrode compared with that of Pd/GC electrode (compare Figs. 5c and 5a). Furthermore, a negative shift of ca. 21 and 40 mV has been noticed in the onset potential (E_{onset}) of FAO at Pd/Ir/GC and Ir/Pd/GC electrodes, respectively. All of that demonstrate the promotion of Ir to Pd for FAO.

Stability of the Pd–based catalysts is another important factor in the practical use of DFAFCs. Fig. 6 shows current transients measured at the Pd/GC, Pd/Ir/GC, and Ir/Pd/GC electrodes in a 0.3 M aqueous solution of FA (pH=3.5) at –0.10 V. Figs. 6a and 6b (at which Pd is the outer most layer) depict the poor stability of the Pd/GC and Pd/Ir/GC electrodes towards FAO, as can be seen from the fast decay of the current with time, which agrees with previous investigations [31]. It is worth mentioning here to say that the current density of the Pd/Ir/GC electrode (Fig. 6b) in the region of activation polarization is higher than that observed at the Pd/GC electrode (Fig. 6a). This matches well with the higher current density of FAO at the Pd/Ir/GC electrode (Fig. 5b) compared with that observed at the Pd/GC electrode (Fig. 5a). However, at the long run, the stability of the Pd/GC electrode was observed to be better than that of the Pd/Ir/GC electrode as can be seen from the final current density values after 1800 s (compare Figs. 6a with 6b). This can be assigned to the difference in the degree of poisoning of the two electrodes where the value of the poisoning rate at the Pd/GC electrode is estimated to be ca. 0.04 % s^{-1} compared with a value of ca. 0.05 % s^{-1} for the Pd/Ir/GC electrode [32].

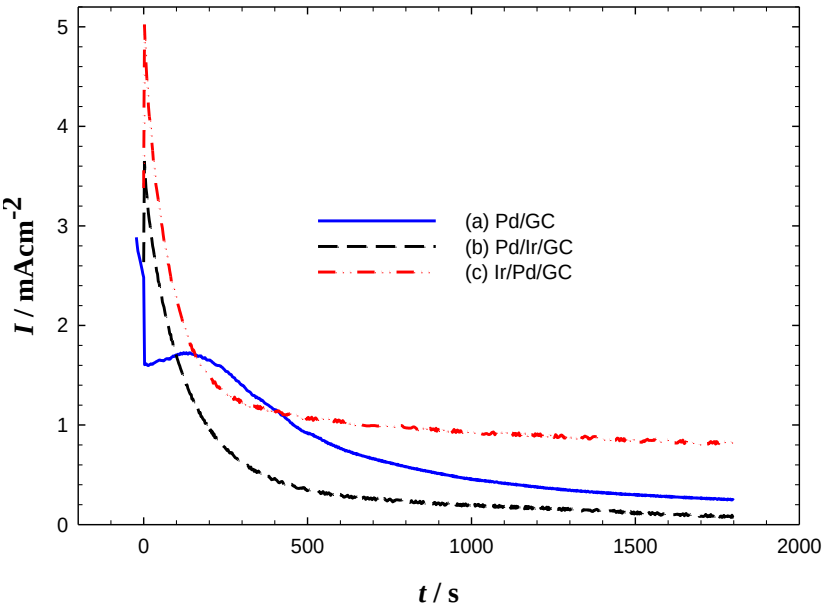

Figure 6. Chronoamperometric curves of (a) Pd/GC, (b) Pd/Ir/GC, and (c) Ir/Pd/GC electrodes in 0.3 M HCOOH (pH = 3.5) at –0.1 V.

Surprisingly, the Ir/Pd/GC electrode exhibits the highest current density in the region of activation polarization and its final current density is 831 μA cm^{-2} compared with 71 and 244 μA cm^{-2} obtained at the Pd/Ir/GC and the Pd/GC electrodes, respectively. Also, the poisoning rate of the Ir/Pd/GC electrode had the lowest value among all the modified electrodes where it could be estimated to be ca. 0.01 % s^{-1}.

Table 1. Summary of the electrochemical measurements obtained from Figs. 5 and 6.

Electrode	I_p (mA cm^{-2})	E_p (mV)	E_{onset} (mV)	I_{pss} (μA)
Ir/GC	–	–	–	–
Pd/GC	2.6	21	–229	58
Pd/Ir/GC	3.3	12	–250	57
Ir/Pd/GC	5.8	8	–269	156

I_p, E_p, E_{onset}: peak current density, peak potential, and onset potential of FAO. I_{pss}: the pseudo-steady state current observed from *i-t* curves.

The remarkable electrocatalytic activity and stability enhancements of the Ir/Pd/GC electrode is thought to come from the electronic enhancement and/or the bi-functional mechanism of Ir to Pd [25,33,34]. Table 1 summarizes the electrochemical measurements obtained from Figs. 5 and 6.

Additionally, some important electrocatalytic parameters, calculated from pseudo-steady state current (I_{pss}), such as time needed to oxidize a complete monolayer of FA and turnover frequency (TOF) have been estimated for the modified electrodes. Utilizing the charge associated with oxidation of a complete monolayer of FA at the Pd/GC and Pd/Ir/GC electrodes, the complete oxidation of a FA monolayer needs 0.91 s and 1.06 s, respectively, on the basis of a two-site adsorption model and the corresponding TOF is estimated to equal 2.2 and 1.9 s^{-1}, respectively [35]. Interestingly, based on the same adsorption model, the complete oxidation of a FA monolayer at the Ir/Pd/GC electrode needs 0.24 s and the corresponding TOF is estimated to equal 8.3 s^{-1}. These parameters could infer about the superior catalytic activity of the as-prepared Ir/Pd/GC electrode.

4. CONCLUSION

A simple modification of Pd–based catalysts with IrNPs could effectively enhance its catalytic activity and stability towards FAO. The deposition order of PdNPs and IrNPs onto the GC influenced, to a great extent, the catalytic efficiency. The highest catalytic activity and stability were obtained at the Ir/Pd/GC electrode (in which IrNPs were partially deposited onto the Pd/GC electrode). The enhancement in the electrocatalytic activity and stability of the Ir/Pd/GC electrode might be attributed to the electronic enhancement and/or the bi-functional mechanism of IrNPs to the Pd–based catalysts.

References

1. M. Carmo, G. Doubek, R.C. Sekol, M. Linardi and A.D. Taylor, *J. Power Sources*, 230 (2013) 169.
2. S. Nishimura, N. Ikeda and K. Ebitani, *Catal. Today*, 232 (2014) 89.
3. A.M. Abdullah, A.M. Mohammad, T. Okajima, F. Kitamura and T. Ohsaka, *J. Power Sources*, 190 (2009) 264.
4. B. Braunchweig, D. Hibbitts, M. Neurock and A. Wieckowski, *Catal. Today*, 202 (2013) 197.
5. M. Bron and C. Roth, in: S.L. Suib (Ed.), Elsevier, Amsterdam, 2013, pp. 271.
6. I.M. Al-Akraa, A.M. Mohammad, M.S. El-Deab and B.E. El-Anadouli, *Chem. Lett.*, 40 (2011) 1374.
7. I.M. Al-Akraa, A.M. Mohammad, M.S. El-Deab and B.E. El-Anadouli, *Int. J. Electrochem. Sci.*, 7 (2012) 3939.
8. G.A. El-Nagar and A.M. Mohammad, *Int. J. Hydrogen Energy*, 39 (2014) 11955.
9. U.B. Demirci, *J. Power Sources*, 169 (2007) 239.
10. X. Wang, J.-M. Hu and I.-M. Hsing, *J. Electroanal. Chem.*, 562 (2004) 73.
11. Y.W. Rhee, S.Y. Ha and R.I. Masel, *J. Power Sources*, 117 (2003) 35.
12. G.A. El-Nagar, A.M. Mohammad, M.S. El-Deab and B.E. El-Anadouli, *Electrochim.Acta*, 94 (2014) 62.
13. G.A. El-Nagar, A.M. Mohammad, M.S. El-Deab, T. Ohsaka and B.E. El-Anadouli, *J. Power Sources*, 265 (2014) 57.
14. C. Rice, S. Ha, R.I. Masel and A. Wieckowski, *J. Power Sources*, 115 (2003) 229.
15. S.D. Han, J.H. Choi, S.Y. Noh, K. Park, S.K.Yoon and Y.W. Rhee, *Korean J. Chem. Eng.*, 26 (2009) 1040.
16. A.S. Bauskar and C.A. Rice, *Electrochim. Acta*, 107 (2013) 562.

17. H. An, L. Pan, H. Cui, B. Li, D. Zhou, J. Zhai and Q. Li, *Electrochim. Acta*, 102 (2013) 79.
18. D.W. Yuan and Z.R. Liu, *J. Power Sources*, 224 (2013) 241.
19. G. Zhang, Y. Wang, X. Wang, Y. Chen, Y. Zhou, Y. Tang, L. Lu, J. Bao and T. Lu, *Appl. Catal. B: Environ.*, 102 (2011) 614.
20. S. Hu, L. Scudiero and S. Ha, *Electrochim. Acta*, 83 (2012) 354.
21. X. Yu and P.G. Pickup, *Electrochem. Commun.*, 11 (2009) 2012.
22. Y.-H. Qin, Y. Jiang, D.-F. Niu, X.-S. Zhang, X.-G. Zhou, L. Niu and W.-K. Yuan, *J. Power Sources*, 215 (2012) 130.
23. G. Chen, M. Liao, B. Yu, Y. Li, D. Wang, G. You, C.-J. Zhong and B.H. Chen, *Int. J. Hydrogen Energy*, 37 (2012) 9959.
24. G.A. El-Nagar, A.M. Mohammad, M.S. El-Deab and B.E. El-Anadouli, *J. Electrochem. Soc.*, 159 (2012) F249.
25. X. Wang, Y. Tang, Y. Gao and T. Lu, *J. Power Sources*, 175 (2008) 784.
26. F. Alardin, H. Wullens, S. Hermans and M. Devillers, *J. Molec. Catal. A: Chem.*, 225 (2005) 79.
27. T. Teranishi and M. Miyake, *Chem. Mater.*, 10 (1998) 594.
28. B. Zhang, D. Ye, J. Li, X. Zhu and Q. Liao, *J. Power Sources*, 214 (2012) 277.
29. S.M. Baik, J. Han, J. Kim and Y. Kwon, *Int. J. Hydrogen Energy*, 36 (2011) 14719.
30. J.-H. Choi, K.-J. Jeong, Y. Dong, J. Han, T.-H. Lim, J.-S. Lee and Y.-E. Sung, *J. Power Sources*, 163 (2006) 71.
31. P. Hong, F. Luo, S. Liao and J. Zeng, *Int. J. Hydrogen Energy*, 36 (2011) 8518.
32. J. Jiang and A. Kucernak, *J. Electroanal. Chem.*, 543 (2003) 187.
33. J. Chen, Y. Li, Z. Gao, G. Wang, J. Tian, C. Jiang, S. Zhu and R. Wang, *Electrochem. Commun.*, 37 (2013) 24.
34. J. Chen, Y. Li, S. Liu, G. Wang, J. Tian, C. Jiang, S. Zhu and R. Wang, *Appl.Surf. Sci.*, 287 (2013) 457.
35. M. Osawa, K. Komatsu, G. Samjeske, T. Uchida, T. Ikeshoji, A. Cuesta and C. Gutierrez, *Angew. Chim. Int. Ed.*, 50 (2011) 1159.